Light Metals 2014
Edited by: John Grandfield
TMS (The Minerals, Metals & Materials Society), 2014

LONG AND SMALL FATIGUE CRACK GROWTH IN ALUMINUM ALLOYS

Anthony Spangenberger[1], Anastasios Gavras[1], Diana Lados[1]
[1] WPI (Worcester Polytechnic Institute), 100 Institute Rd.; Worcester, MA 01609, USA

Keywords: Cast and Wrought Aluminum Alloys, Small and Long Fatigue Crack Growth, Microstructure

Abstract

Fatigue crack growth (FCG) studies at various stress ratios (R=0.1, 0.5, 0.7) were performed on solution-strengthened (cast A535) and precipitation-strengthened (cast A356, 319, A390 and wrought 6061) aluminum alloys. Microstructures were altered through processing, chemistry, and heat treatment (T4, T6, T7) to shed light on the effects of various intrinsic material characteristic features on FCG (e.g. Si amount/type/morphology, grain size, secondary dendrite arm spacing, precipitate type/size). In this context, mechanisms of long and small fatigue crack growth at the microstructural scale of the studied alloys were identified, and loading-microstructure-damage mechanisms design maps were created. The differences in FCG responses between long, physically-small, and microstructurally-small cracks were systematically evaluated, and an original fracture mechanics – materials science combined model that accounts for these differences was developed, having both material and crack size dependency. Examples of the use of this integrated methodology for design and fatigue life predictions will also be given.

Introduction

Aluminum alloys are a desirable choice for automotive and aerospace structural components due to their low density and good strength. The integrity of these structures highly depends on the material's FCG resistance. Although extensive research has been done on FCG, crack propagation mechanisms at the microstructural scale of the materials are still not well understood, and the available data are often limited. The goal of this study is to fill this knowledge gap by investigating long and small FCG in various aluminum alloys used in structural applications and providing design guidelines for enhanced FCG performance.

Materials, Microstructures, and Experimental Procedure

Cast and wrought aluminum alloys (A535-F, A356-T6, 319-T6, A390-T6, and 6061-T6) were investigated in this study. Each material, composition, and processing condition was designed to isolate specific microstructural features of the alloy and study their individual and combined effect on fatigue crack growth. Secondary microstructural phases and the grain structure of all studied alloys are shown in Fig. 1. Those materials which will be discussed here are:

1. Cast Al-7% Mg: A535; two grain sizes (75 and 450 μm), solution hardened; as-cast (F condition)
2. Hypo-eutectic cast Al-7%Si-Mg: A356; two SDAS (45 μm and 90 μm) & two grain sizes (500 μm and 1300 μm); unmodified and modified eutectic Si structure; Mg-Si precipitation hardened; T6
3. Hypo-eutectic cast Al-7%Si-Cu-Mg: 319; 90 μm SDAS and 1300 μm grain size; unmodified eutectic Si structure; Al-Cu & Al-Cu-Mg-Si precipitation hardened; T6
4. Hyper-eutectic cast Al-17%Si-Cu-Mg: A390; 1300 μm grain size; unmodified eutectic and primary Si structure; Al-Cu & Al-Cu-Mg-Si precipitation hardened; T6
5. Rolled Al-Mg-Si: 6061; recrystallized "pancake" grain structure (1:3 ratio, 180 μm x 550 μm); Mg-Si precipitation hardened; T6

Long fatigue crack growth tests were conducted on all alloys using compact tension, C(T), specimens with dimensions 63.5 mm x 61 mm x 10 mm. Constant stress ratio tests (R=0.1, 0.5, and 0.7) and constant K_{max} tests with variable stress ratio were conducted. Small fatigue crack growth experiments were run

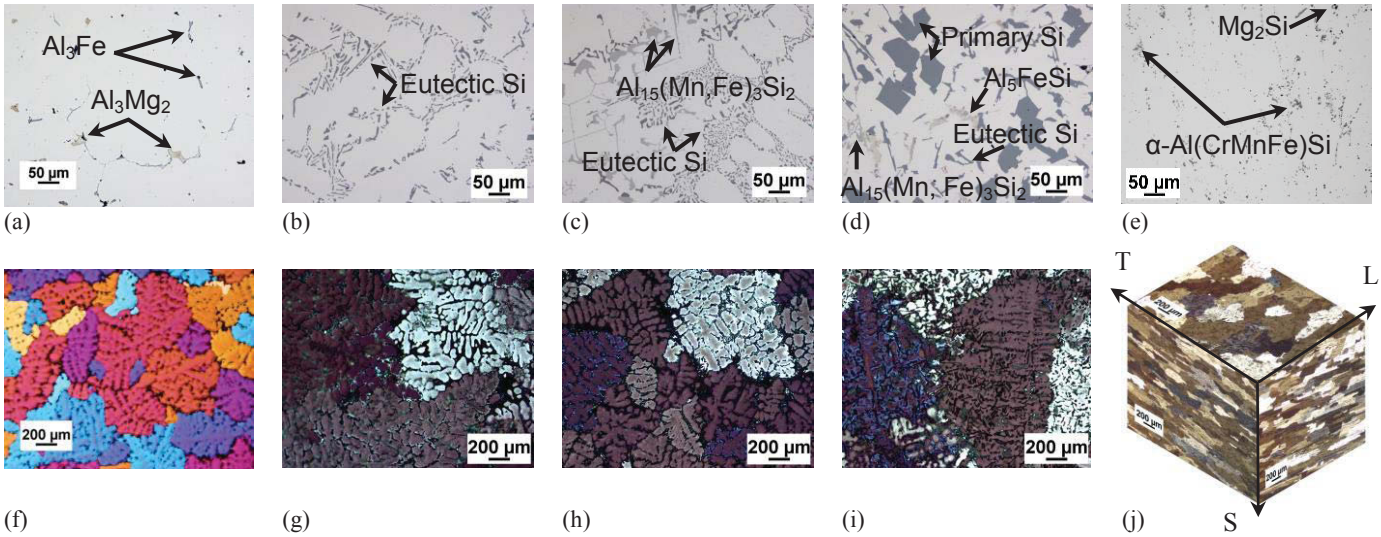

Figure 1. (a-e) Microstructural phases and (f-j) grain structures of A535-F, A356-T6, 319-T6, A390-T6, and 6061-T6 alloys.

using corner flaw tension, CF(T), and surface flaw tension, SF(T), specimens. The specimens had a gage cross section of 10 mm x 5 mm. The notch size varied from 75 μm to 300 μm. All small crack growth experiments were performed at R=0.1, and only the results for the A535 alloys will be presented and discussed here. Both long and small growth tests were run at room temperature, relative humidity 20-50%, and cyclic frequency 20 Hz.

Results and Discussion

Fatigue Crack Growth Response at R=0.1 and Microstructural Mechanisms.

Long FCG data for all materials at R=0.1 are shown in Fig. 2. The highest long crack growth threshold is observed in the case of the 3xx-T6 cast alloys followed by the 6061-T6 and A535-F alloys, which have similar thresholds. The 6061-T6 alloy exhibits the highest resistance to crack growth and the highest fracture toughness. For the cast 3xx alloys, it was observed that increased Si content (17% in A390 versus 7% in 319 and A356) results in lower crack growth resistance and lower fracture toughness, as the alloys become more brittle. Comparisons within 3xx alloys are shown in Fig. 3, to illustrate the individual role of microstructural features (SDAS, Sr-modification, and grain size) with other variables maintained constant. Secondary dendrite arm spacing is shown to affect the low cycle, Region III, behavior where lower SDAS increases the fracture toughness. This is attributed to the greater yield strength associated with lower SDAS materials, and consequent constraint of the plastic zone at high ΔK. At equivalent driving forces, the material with the smaller plastic zone can sample less second phase particles and is statistically less likely to encounter preferential particles for crack advance. It can be seen that Region II and III crack growth resistance are both correlated with the degree of Si modification. A lesser extent of Si modification is associated with higher crack propagation rates in upper Region II and Region III, and lower fracture toughness. This effect is associated with Si particle geometry, as angular particles create stress concentrations that facilitate crack advance whereas Sr-modified particles homogenize stresses such that driving forces are minimized. Lastly, lower grain size is associated with a lower crack growth threshold. This effect is due to roughness-induced closure, as the crack follows a more tortuous path in the higher grain size material, leaving a greater number of interfering asperities in the crack wake.

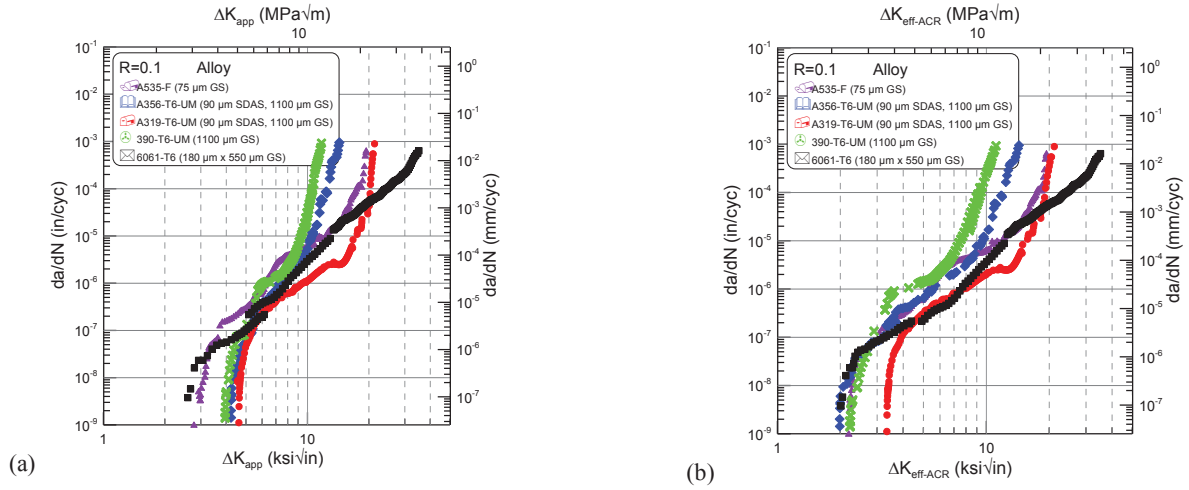

Figure 2. Long fatigue crack growth curves of all studied alloys at R=0.1: (a) data before closure corrections and (b) data after adjusted compliance ratio (ACR) [1] closure corrections.

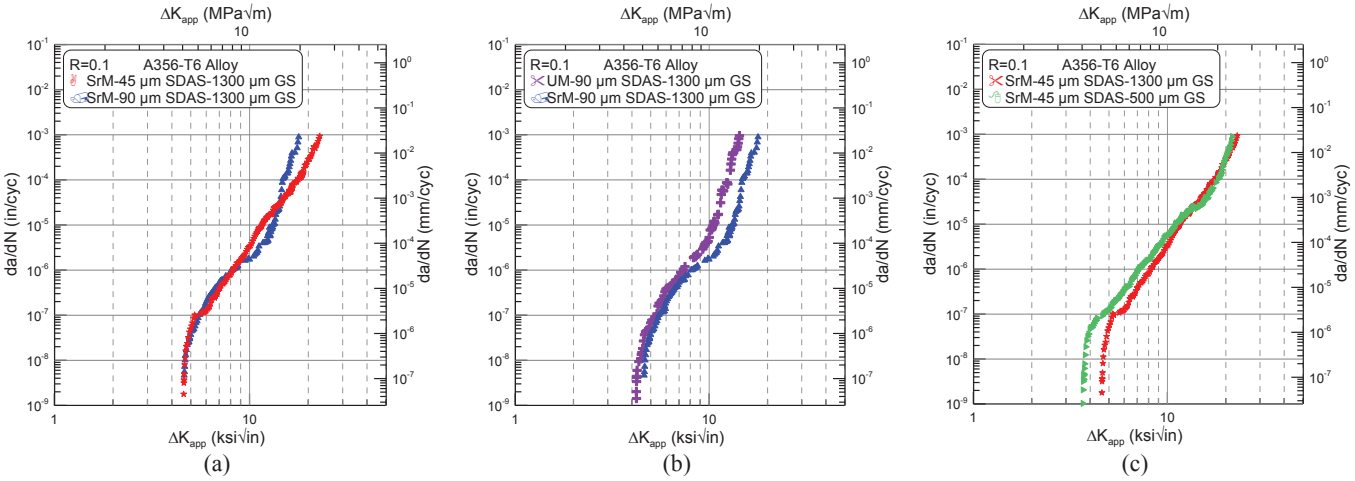

Figure 3. Long fatigue crack growth curves comparing the effect of microstructural features: (a) 45 μm vs. 90 μm SDAS, (b) Sr-unmodified vs. Sr-modified eutectic Si, (c) 500 μm vs. 1300 μm grain size.

Fracture surface profiles for each material at R=0.1 are presented in Fig. 4. For the A535 alloy, at low ΔK values, crack propagation is transgranular, and at higher ΔK, a mixed mode of crack propagation is observed until the change to an intergranular mode in Region III. The crystallographic mode of crack advance produces a rough crack path in the near-threshold regime, and grain-size-dependent roughness-induced closure mechanisms dictate the long crack growth threshold. Crack propagation in the A356 and 319 alloys occurs primarily through the α-Al matrix at low ΔK values and shows an increasing tendency for interactions with eutectic Si particles in upper Region II and Region III, as the plastic zone becomes large enough to sample a significant number of weakened and/or preferentially located Si particles (~200 μm, or 2-3 times the SDAS), Figs. 5(a-f). The A390 alloy also shows a preference for interactions with the primary and eutectic Si phases with increasing crack driving force. Primary Si particles in the A390 alloy tend to form colonies at grain junctions, which create stress concentrations and increase the likelihood of interactions with the crack, thus increasing the crack propagation rates and lowering the fracture toughness relative to the A356 and 319 alloys [2,3], Figs. 5(g-i). In 6061-T6, the main mode of crack advance is transgranular. Secondary Fe phases deflect the crack, while incoherent dispersoids in these Al-Mg-Mn-Si alloys suppress intergranular fracture by reducing strain concentration at the grain boundaries [4]. Thus, microstructural constituents within the matrix, smaller than the grain size, control the crack growth process in this alloy. Based on fractographic observations from tests at various stress ratios, design maps that illustrate the fatigue crack growth mechanistic changes at the microstructural scale were constructed in terms of the two main crack tip driving forces, $\Delta K_{eff\text{-}ACR}$ and K_{max} (Fig. 6).

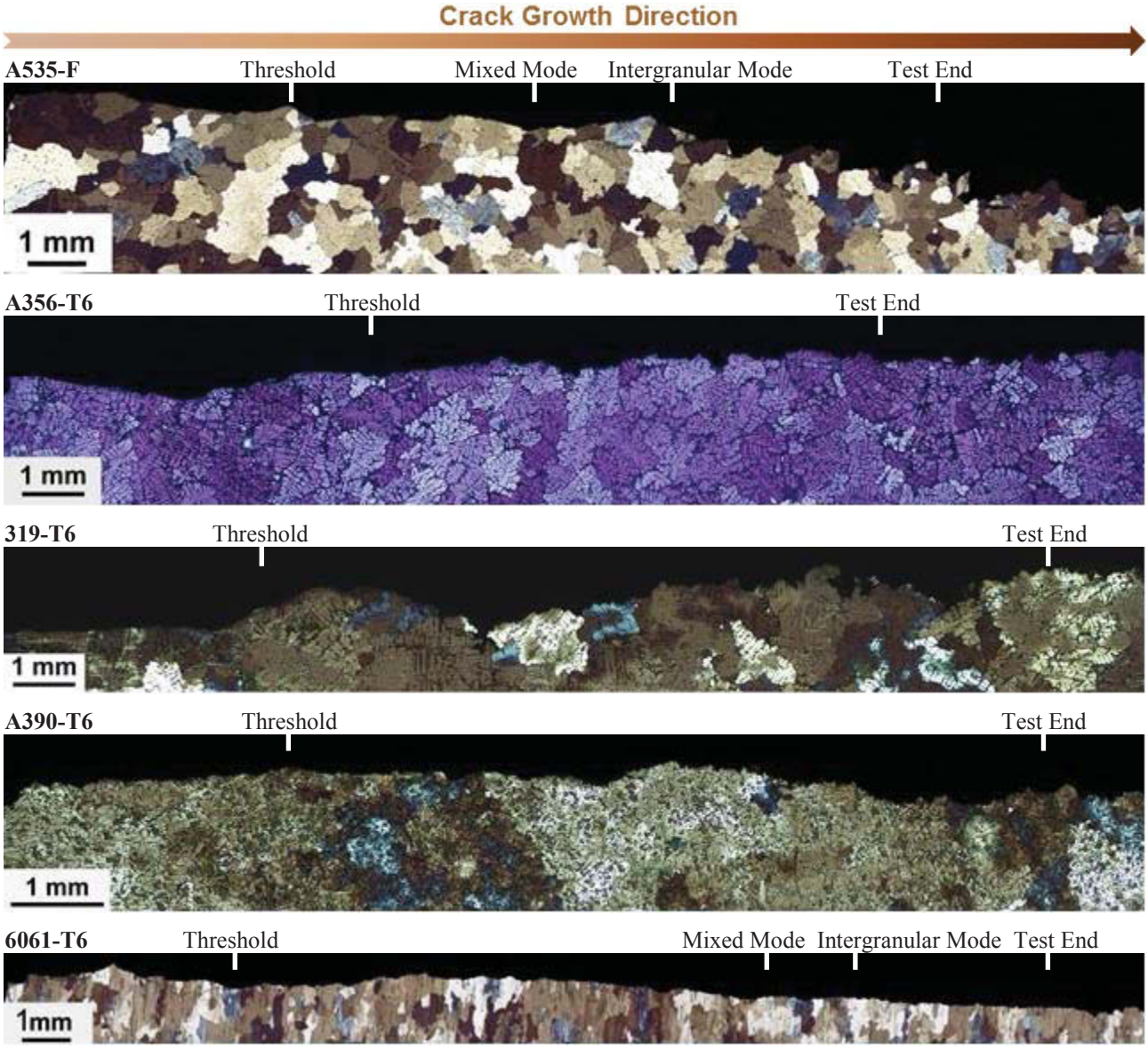

Figure 4. Fracture surface profiles at R=0.1 for all alloys (A535-F, A356-T6, 319-T6, A390-T6, and 6061-T6).

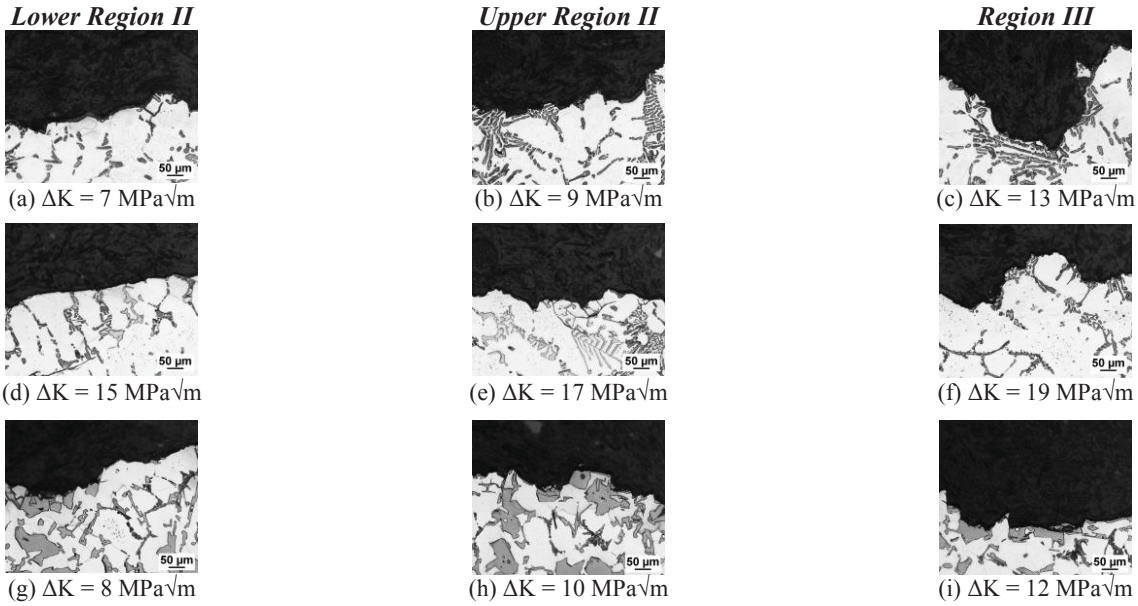

Figure 5. Fracture surface profiles in Regions II and III for 3xx cast alloys tested at R=0.1; (a-c) A356-T6, (d-f) 319-T6, and (g-i) A390-T6

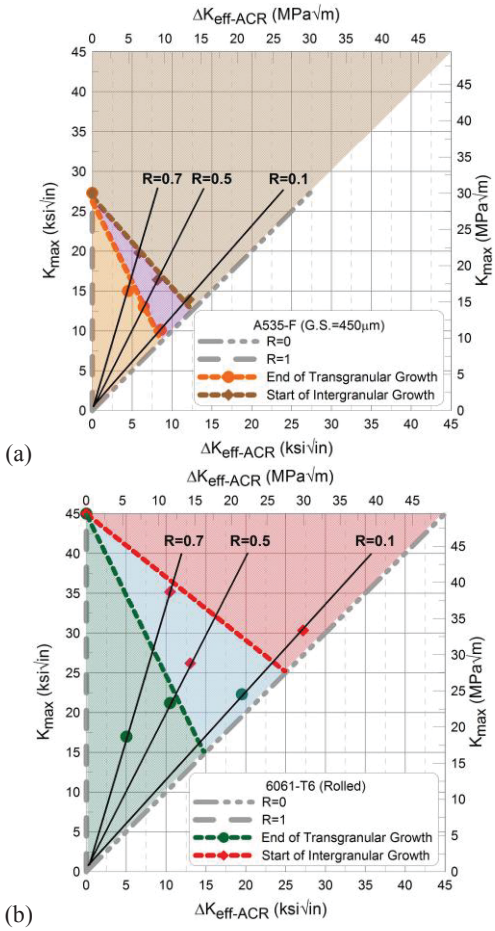

Figure 6. Fatigue crack growth mechanisms design maps for (a) A535-F and (b) 6061-T6 alloys; these maps uniquely combine metallurgical and mechanical parameters critical to material and component design and inspection schedules.

Stress Ratio, Initial Crack Size, and K_{max} Effects on Fatigue Crack Growth Data and Design Curves.

In Figs. 7(a,b), stress ratio, K_{max}, and microstructurally small crack effects are shown for the cast A535-F alloy. Small cracks have lower thresholds and higher growth rates compared to long cracks. Higher stress ratios, R, result in lower thresholds and higher growth rates. The long crack growth data were normalized to incorporate K_{max} effects, Fig. 7(c), and closure free, physically small crack growth data were predicted in Fig. 7(d) based on the mean normalized curve; Eqs. 1 and 2, were used to calculate K_{norm} and $\Delta K_{eff\text{-}norm}$. To incorporate microstructural effects, a new model was developed, Eq. 3, using K_{norm} and Ω, a microstructure-dependent term. The Ω term is a function of crack length, *a*, local and bulk properties, and area fractions of the material's characteristic microstructural features, Eq. 4.

$$K_{norm} = \Delta K_{eff\text{-}ACR}^{(1-n)} \times K_{max}^{n} \quad (1)$$

$$\Delta K_{eff\text{-}norm} = K_{norm} \times (1-R)^{n} \quad (2)$$

$$\Delta K_{microstructurally\text{-}small} = K_{norm} \times (1-R)^{n} \times \Omega \quad (3)$$

$$\Omega = \frac{a_{initial} + \sum_{i=1}^{n} \Delta a_i}{a_{transition}} \times \left[\sum_{j=1}^{n} AF_j \times \frac{\sigma_{Y(local)_j}}{\sigma_{Y(bulk)}} \right] \quad (4)$$

To exemplify the use of the model, a two-dimensional flaw with an initial size, $a_{initial}$, is considered in the microstructural domain, Fig. 8(a). After *N* number of cycles at a given crack propagation rate, the flaw will advance by an increment of Δ*a*, which when added to the initial flaw size, $a_{initial}$, yields the current crack length, $a_{current}$. The current crack length, is then divided by the transition crack length, $a_{transition}$, to give a dimensionless value for the crack length term in Eq. 4. Within the crack extension increment, Δ*a*, certain microstructural features are enveloped. It is the resistance of these microstructural features that determines the crack's advance. Thus, in the property term, the relative area fractions of the microstructural features encountered within the

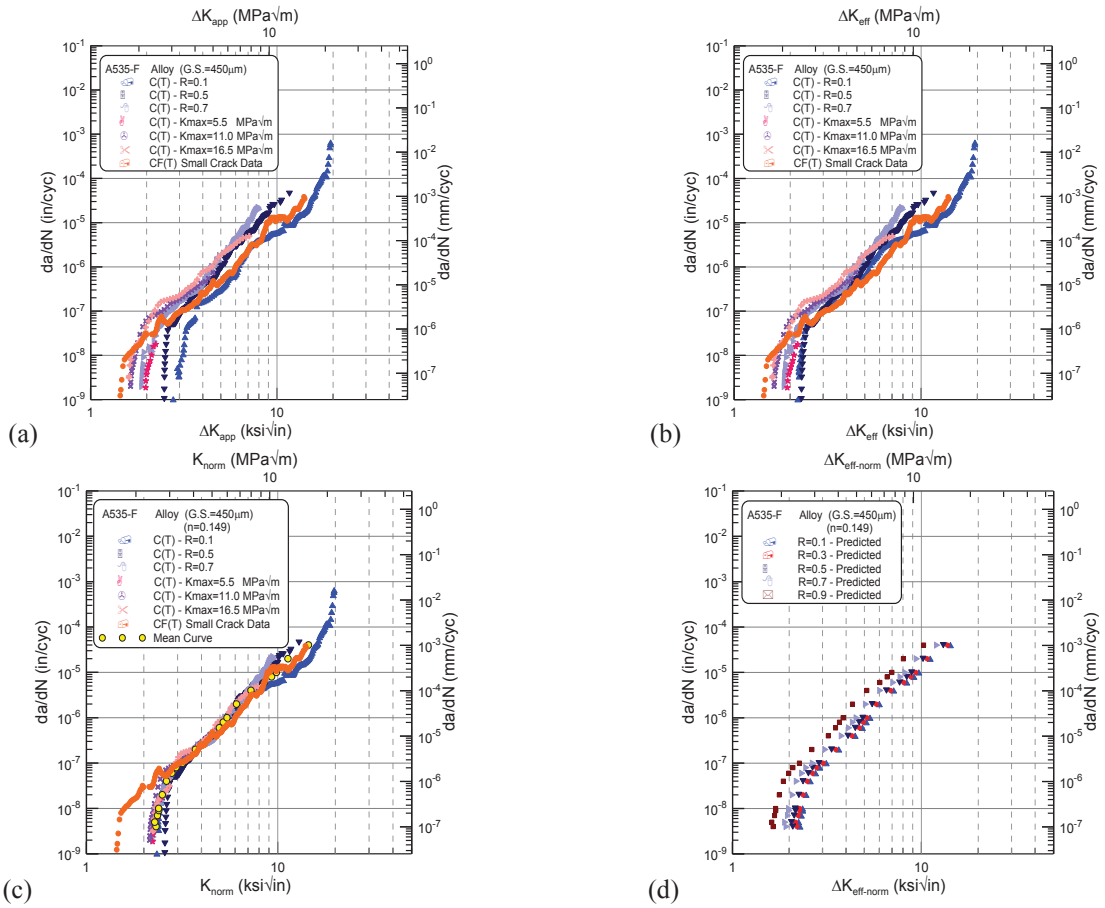

Figure 5. (a,b) Stress ratio, K_{max}, and small crack effects; (c,d) data normalization and prediction.

crack extension increment, Δa, are multiplied by their local resistance to yield, $\sigma_{Y(local)}$, normalized by the bulk yield strength, $\sigma_{Y(bulk)}$. The product of the crack length and property terms provides a "microstructural correction", which applied to the physically small FCG data will provide the microstructurally small FCG behavior for the crack propagation rate of interest. When the crack length term approaches unity, the microstructurally small character of the crack is lost, and the iterative corrective process stops. The results of the corrective model are shown in Fig. 8(b); good agreement is observed between the calculated and experimental microstructurally small FCG behavior.

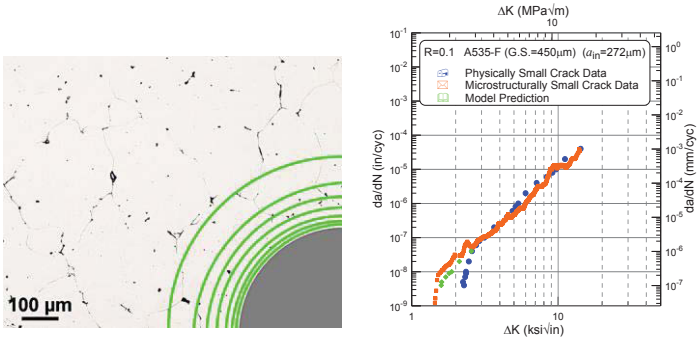

Figure 6. (a) Microstructural domain used to exemplify the application of the model and (b) comparison between experimental and predicted data in the A535-F alloy.

Conclusions

The long fatigue crack growth behavior in A535 is affected by grain size, while the crack growth in 3xx and 6061 alloys is influenced by features within the grain structure. Stress ratio and initial flaw size have significant effects on FCG behavior. Two-parameter ($\Delta K_{eff\text{-}ACR}$ and K_{max}) maps were created as tools to predict the microstructural response under given dynamic loading conditions, optimize materials and processes for FCG resistance, and properly select the inspection intervals on actual components. A model that predicts the response of microstructurally small fatigue cracks was developed, and the predicted and experimental data are in good agreement.

References

[1] J.K. Donald, G.H. Bray and R.W. Bush, in: Fatigue and Fracture Mechanics 29, T.L. Panontin and S.D. Sheppard (eds.), ASTM STP 1332, Philadelphia, PA: ASTM, 1999, pp. 674-695.

[2] K. Gall, N. Yang, M. Horstemeyer, D.L. McDowell, and J. Fan: Fatigue & Fracture of Engineering Materials & Structures, Vol. 23 (2000), pp. 159-172.

[3] K.S. Chan, P. Jones, Q. Wang: Materials Science and Engineering, Vol. 341 (2001), pp. 18-34.

[4] J.M. Dowling and J.W. Martin: Acta Metallurgica, Vol. 24 (1976), pp. 1147-1153.